Journal of Alloys and Compounds 509 (2011) 9071–9075

Contents lists available at ScienceDirect

Journal of Alloys and Compounds

journal homepage: www.elsevier.com/locate/jallcom

Full X–Ku band microwave absorption by Fe(Mn)/Mn_7C_3/C core/shell/shell structured nanocapsules

Xianguo Liu [a,b], Siu Wing Or [b,*], S.L. Ho [b], Chi Chuen Cheung [b], Chung Ming Leung [b], Zheng Han [a], Dianyu Geng [a], Zhidong Zhang [a]

[a] Shenyang National Laboratory for Materials Science, Institute of Metal Research and International Centre for Materials Physics, Chinese Academy of Sciences, Shenyang 110016, PR China

[b] Department of Electrical Engineering, The Hong Kong Polytechnic University, Hung Hom, Kowloon, Hong Kong

ARTICLE INFO

Article history:
Received 19 May 2011
Received in revised form 7 June 2011
Accepted 7 June 2011
Available online 6 July 2011

Keywords:
Carbon
Complex permeability
Complex permittivity
Electromagnetic wave absorption
Nanocapsules
Reflection loss

ABSTRACT

New type of Fe(Mn)/Mn_7C_3/graphite nanocapsules was prepared by a modified arc discharge technique in ethanol vapor, with Fe(Mn) solid solution nanoparticles as the core, Mn_7C_3 as the inner shell, and graphite as the outer shell. The Cole–Cole semicircle approach was adopted to explain the ternary dielectric resonance, due to a cooperative consequence of the core/shell/shell interfaces and the dielectric Mn_7C_3 and C shells. A remarkable increase in the anisotropy energy led to a shift in the natural resonance frequency to 6.6 GHz. Dielectric losses come from the ternary dielectric resonance while magnetic losses were from the magnetic natural resonance. An optimal reflection loss (RL) of −142.1 dB was observed at 12 GHz for 5.0 mm thickness layer. RL exceeding −10 dB was obtained at 6.6–18 GHz for 1.4 mm thickness, covering the whole X band (8–12 GHz), Ku band (12–18 GHz), and some of C band (6.6–8.0 GHz). RL exceeding −20 dB was found at 6–10.6 GHz for 2.2 mm thickness.

1. Introduction

During the past few years, there has been a growing and widespread interest in microwave absorbing materials due to their military and civil applications such as stealth defense system, microwave interference protection, and microwave darkroom [1–15]. Recent developments in microwave absorber technology have resulted in materials that can effectively reduce the reflection of electromagnetic signals on the one hand, and have good physical performance and lower production cost on the other hand [4–15]. It is well known that reflection loss (RL), in decibels (dB), can be used to characterize the absorption properties of microwave absorbing materials. According to the transmission line model based on the assumption that the dielectric permittivity and magnetic permeability are intrinsic properties of the materials [9–15], RL of a metal-backed microwave absorbing layer is

$$\mathrm{RL} = 20\ \log_{10}\left(\frac{jZ\tanh(kd)-1}{jZ\tanh(kd)+1}\right) \quad \text{with} \quad Z=\sqrt{\frac{\mu_r}{\varepsilon_r}} \quad \text{and}$$

$$k=\frac{2\pi f}{c}\sqrt{\mu_r\varepsilon_r}. \tag{1}$$

Here, the materials constants $\mu_r = \mu' - j\mu''$ and $\varepsilon_r = \varepsilon' - j\varepsilon''$ are the complex permeability and complex permittivity, respectively, d is the absorption layer thickness, and f is the frequency of incident wave. According to Eq. (1), an ideal absorber must fulfill the relation that $\varepsilon_r = \mu_r$, indicating the full absorption of microwave. One important factor which should be taken into account is how to effectively match the permittivity and the permeability. For traditional materials such as ferrites and ferromagnetic metals, the values of μ_r are much smaller than those of ε_r in microwave band, leading to poor microwave absorption properties. Nanoscale composites of transition metals and dielectric materials, especially core–shell structures, tend to exhibit good microwave absorption properties (such as high absorption frequencies, broad absorption bands, and thin layer thicknesses) because of the good electromagnetic (EM) matching of the special core/shell microstructures [16–19]. In addition, for core–shell structured nanocapsules, the values of the dielectric permittivity of shell and those of the magnetic permeability of the core can be easily altered to achieve the maximal absorption of the microwave energy.

* Corresponding author at: Department of Electrical Engineering, The Hong Kong Polytechnic University, Hung Hom, Kowloon, Hong Kong. Tel.: +852 34003345; fax: +852 23301544.
E-mail address: eeswor@polyu.edu.hk (S.W. Or).

0925-8388/$ – see front matter © 2011 Elsevier B.V. All rights reserved.
doi:10.1016/j.jallcom.2011.06.031

Among these nanocomposites, Fe-based nanocapsules are of great interest due to their typical ferromagnetic characteristics and potential application in microwave absorption [6,7,9–11,13,15]. Some Fe-based nanocapsules, including Fe/C, Fe/SiO_2, Fe/ZnO, FeCo/Al_2O_3, Fe(Mn)/ferrite[16,19–23], etc. have been prepared and widely been studied. The complex permittivity and complex permeability spectra show that the absorption performance of those Fe-based nanocapsules is better than that of the corresponding NI-based nanocapsules [24]. However, the synthesis, morphology, and materials constants in the core–shell–shell structured nanoparticles of Fe have seldom been reported. In this work, core–shell–shell Fe(Mn)/Mn_7C_3/C nanocapsules are prepared and their complex permittivity, complex permeability, and microwave absorption are investigated in the frequency range of 2–18 GHz.

2. Experimental

The Fe(Mn)/Mn_7C_3/C nanocapsules were prepared by a modified arc-discharge technique in ethanol vapor, which was described in detail in our previous work [25–29]. In brief, a $Fe_{99}Mn$ (at.%) ingot served as the anode, while the cathode was a carbon needle. The anode target was placed into a water-cooled carbon crucible. After the chamber was evacuated in a vacuum of 5.0×10^{-3} Pa, liquid ethanol of 40 ml was introduced into the chamber together with pure argon of 1.6×10^4 Pa and hydrogen of 0.4×10^4 Pa. The arc-discharge current was maintained at 100 A for 8 h to evaporate $Fe_{99}Mn$ ingot sufficiently. Then, the products were collected form depositions on the top of the water-cooled chamber, after passivated for 24 h in argon.

The morphology and microstructure of the nanocapsules were observed by a high-resolution transmission electron microscope (HRTEM JEOL-2010) with emission voltages of 200 kV. Toroidal specimens for microwave measurements between 2 and 18 GHz using an Agilent 8722 ES network analyzer (VNA) with a transverse EM mode were prepared by mixing 40 wt.% Fe(Mn)/Mn_7C_3/C nanocapsules in a paraffin matrix. The complex permittivity and complex permeability were calculated from the *S*-parameter tested by the calibrated VNA, using a simulation program for the Reflection/Transmission Nicolson–Ross model.

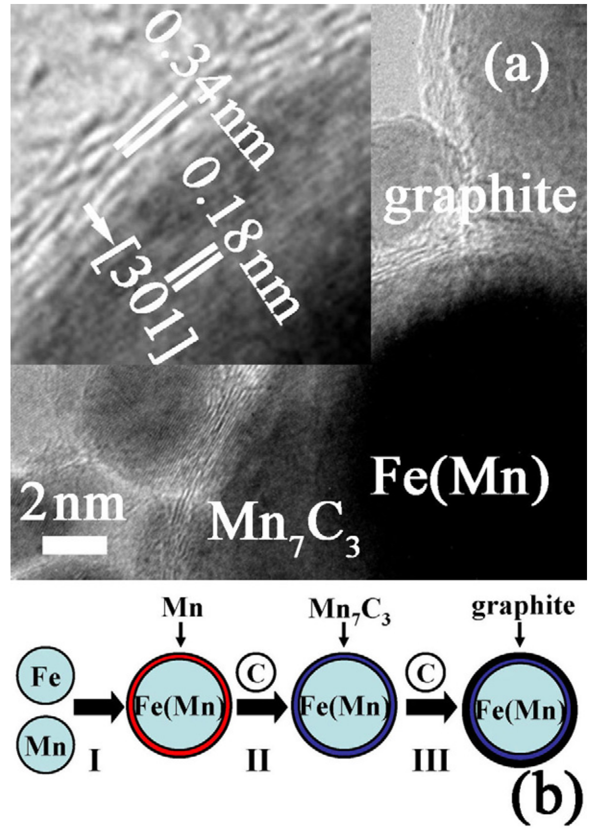

Fig. 1. (a) TEM image of the Fe(Mn)/Mn_7C_3/C nanocapsules. The inset shows the HRTEM image of double shells in nanocapsules. (b) A schematic illustration of the formation mechanism of the Fe(Mn)/Mn_7C_3/C nanocapsules.

3. Results and discussion

The HRTEM image is presented in Fig. 1(a). Fig. 1(a) shows that the nanocapsules are spherical about 5–30 nm in diameter, with well-defined core/shell/shell structures containing Fe(Mn) nanoparticles as cores. As shown in inset of Fig. 1(a), the *d*-spacing of 0.34 nm in onion-like outer shell corresponds to the (0 0 2) plane of graphite, and the characteristic lattice fringes {3 0 1} plane with *d*-spacing of 0.18 nm in inner shell correspond to Mn_7C_3. A schematic illustration of the formation mechanism of the Fe(Mn)/Mn_7C_3/C nanocapsules is shown in Fig. 1(b). In the arc-discharge process, Fe and Mn atoms evaporated from the bulk $Fe_{99}Mn$ alloy anodes to the chamber, in which the atoms with a high activity reacted rapidly and nucleated through the rapid energy exchange [16–18]. Fe atoms and Mn atoms bump up each other to be Fe(Mn) solid solution [23]. In essence, the boiling point (or evaporation pressure) of metals determines the condensed priority of evaporated atoms. With its boiling point of 3135 K, Fe(Mn) solid solution is more easily condensed than Mn with a boiling point of 2335 K. Due to the adsorption effect of large surface, the other Mn atoms can be deposited on the surface of Fe(Mn) solid solution. The C from the decomposition of ethanol is easily reacted with Mn shells in Fe(Mn)/Mn nanocapsules to form Mn_7C_3 shells due to the high surface energy from the size effect. It is noteworthy that only Mn_7C_3 binary compound appears as the shell due to the fact that Mn_7C_3 is a stable phase with the highest decomposition temperature in the Mn–C phase diagram. The left C atoms are absorbed by Fe(Mn)/Mn_7C_3 nanocapsules and subsequently condense to form a graphite layer on the surface[4,17–19]. Fig. 2(a) shows the frequency dependence of the real part (ε') and imaginary part (ε'') of the relative complex permittivity of the paraffin-Fe(Mn)/Mn_7C_3/C nanocapsules composite in the 2–18 GHz range. It can be seen that both ε' and ε'' have fluctuating behavior, which can be attributed to the displacement current lag at the core/shell interface [19,23]. ε' decreases from 12.1 to 9.2, while ε'' fluctuates between 0.38 and 0.55, with the maximum value of about 0.55 around 4 GHz. The Fe(Mn) cores are encapsulated by the dielectric Mn_7C_3 shells and the C shells and well dispersed, which cause high resistivity for the Fe(Mn)/Mn_7C_3/C nanocapsules. This high resistivity gives rise to a small value of the ε'', according to the free-electron theory [19,21–23]. In general, ε' is mainly related to polarization, and ε'' implies the dielectric loss in the metal particles. In the metal-based composites, two kinds of mechanisms of polarization have been reported; space charge polarization and dipole polarization. The former is proved to be only distinct in micro-scaled metal-based composites and reduces with decreasing particle size of the composites at high frequency, while the latter is dominant in the permittivity of the core/shell-type metal-based nanoparticles [23,24].

According to the Debye dipolar relaxation expression, $(\varepsilon' - \varepsilon_\infty)^2 + (\varepsilon'')^2 = (\varepsilon_s - \varepsilon_\infty)^2$, where ε_s and ε_∞ are stationary dielectric constant and optical dielectric constant, respectively, and the plot of ε' versus ε'' would be a single semicircle, which is usually defined as the Cole–Cole semicircle [30]. It is worthy to note that the composite presents a clear segment of three semicircles in Fig. 2(b), suggesting the existence of ternary dielectric relaxation processes, while each semicircle corresponds to a Debye dipolar relaxation. During the activation of an EM wave, a redistribution process of the charges occurs periodically in Fe(Mn) cores, Mn_7C_3 shells, and C shells [30,31]. As a result, apart form the dielectric relaxation of the Mn_7C_3 and C shells, an additional interfacial relaxation between the Fe(Mn) cores and the Mn_7C_3 shells is present because a complete core/shell interface is constructed

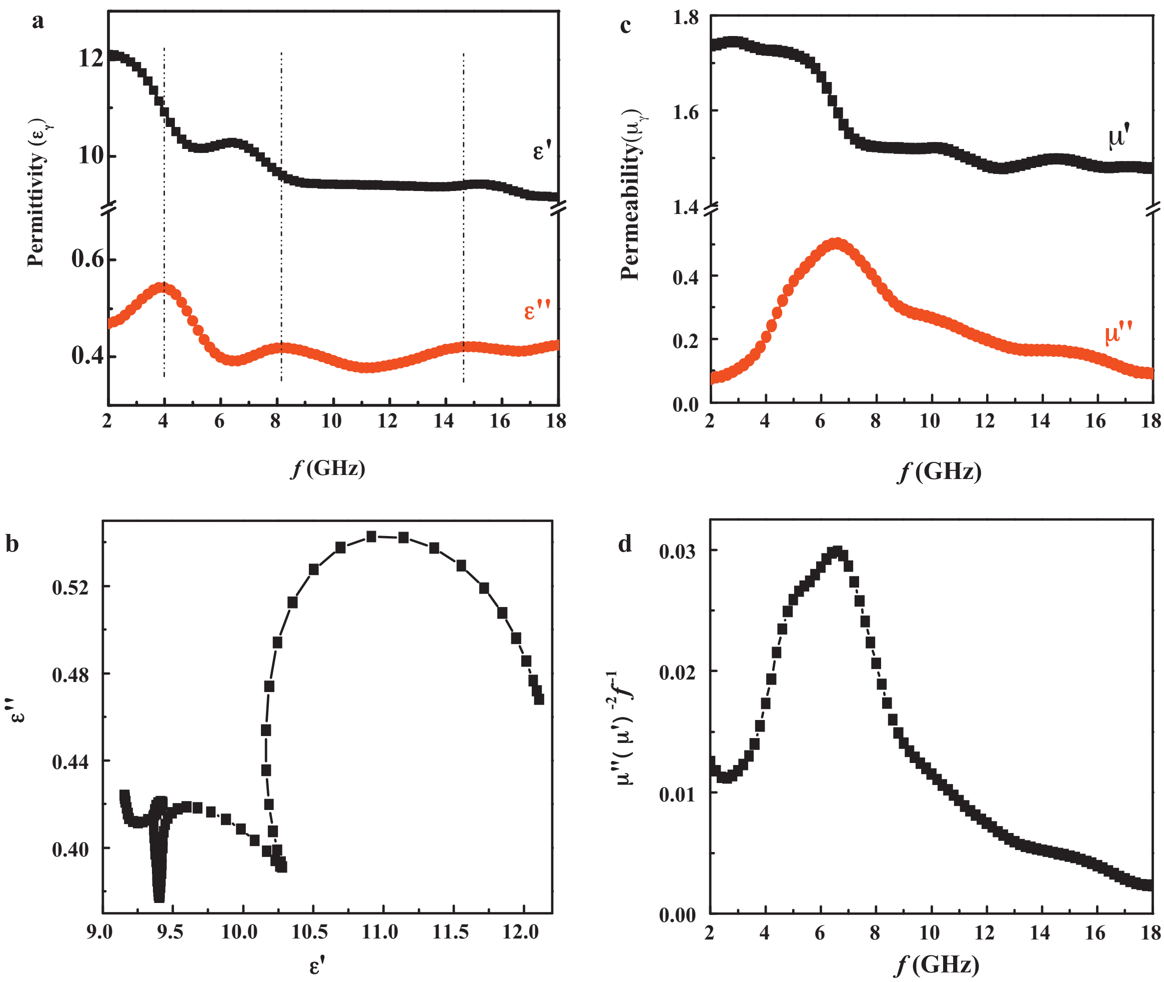

Fig. 2. (a) Relative complex permittivity and (c) relative complex permeability as a function of frequency. (b) Typical Cole–Cole semicircles and (d) values of $\mu''(\mu')^{-2}f^{-1}$ as a function of frequency for Fe(Mn)/Mn_7C_3/C nanocapsules–paraffin composites.

[31]. The interfacial relaxation between the Mn_7C_3 shells and the C shells is absent due to the dielectric properties of Mn_7C_3 and C. The ternary dielectric losses are therefore achieved for the Fe(Mn)/Mn_7C_3/C nanocapsules.

The real part (μ') and imaginary part (μ'') of the relative permeability are plotted in Fig. 2(c) in the frequency range between 2 and 18 GHz. μ' retains an approximately constant value (≈1.74) between 2 and 5.4 GHz, then abruptly decreases from 1.72 at 5.4 GHz to 1.52 at 7.6 GHz, and slowly decreases to 1.48 at 18 GHz. However, μ'' varies with the frequency and presents a broad peak at 4–9 GHz, with the maximum value of 0.5 at 6.6 GHz. This implies the occurrence of natural resonance in the Fe(Mn)/Mn_7C_3/C nanocapsules [4,7–10]. The contributors to magnetic losses, such as magnetic hysteresis, domain-wall displacement, and eddy-current loss, can be excluded from the present nanocapsules. The hysteresis loss can be negligible in a weakly applied field, which is mainly caused by the time lags of the magnetization vector behind the external EM-field vector [30,31]. Because the size of the Fe(Mn)/Mn_7C_3/C nanocapsules can be compared with a single magnetic domain, the contribution of the domain-wall displacement that only occurs in multidomain magnetic materials can be excluded. According to the skin-effect criterion, if the magnetic losses result from eddy-current loss, the values of $\mu''(\mu')^{-2}f^{-1}$ should be constant when frequency is varied [30,31]. As shown in Fig. 2(d), the values of $\mu''(\mu')^{-2}f^{-1}$ remarkably exhibits a broad peak at 4–10 GHz. Therefore, the magnetic losses in the present nanocapsules caused are mainly by the natural resonance. Similar phenomenon has been analyzed in detail in our previous work [18,31].

Furthermore, the magnetic resonance frequency (f_r) is dependent on the particle's radius. Because of the size effect, the anisotropy energy of small particles will be significantly increased due to the enhanced surface anisotropy, according to a simple model ($K_{eff} = K_V + 6K_S/d$) [19,23,32]. K_V and K_S refer to the volume and surface contributions to anisotropies, respectively [2,9]. In addition, a large number of lattice defects, interior stress, etc., resulting from the non-equilibrium solid solution of Mn atoms in Fe particles, can also bring an increase in the effective anisotropy field. Consequently, the effective anisotropy field $H_{eff} = 4\left|K_{eff}\right|/(3\mu_0 M_S)$ will be increased [23,32,33]; it is well known that f_r is related to its effective anisotropy field (H_{eff}) by $2\pi f_r = rH_{eff}$, where r is the gyromagnetic ratio. Bulk α-Fe has a K_{eff} of 4.81×10^4 J m^{-3}, and it can be estimated that f_r of bulk α-Fe is about several megahertz [23]. However, the resonance frequency of the Fe(Mn)/Mn_7C_3/C nanocapsules is at 6.6 GHz, which indicates a remarkable increase in the anisotropy energy of the Fe(Mn)/Mn_7C_3/C nanocapsules.

To further examine the microwave absorption abilities of the Fe(Mn)/Mn_7C_3/C nanocapsules, RL as a function of absorbing thickness *d* and frequency *f* were calculated, as shown in Fig. 3, according to Eq (1). The optimal RL or the dip in RL corresponds to the occurrence of the maximum absorption or the minimal reflection of the microwave power for the particular thickness [34]. BW_{-10} is defined as the frequency difference between points where RL value

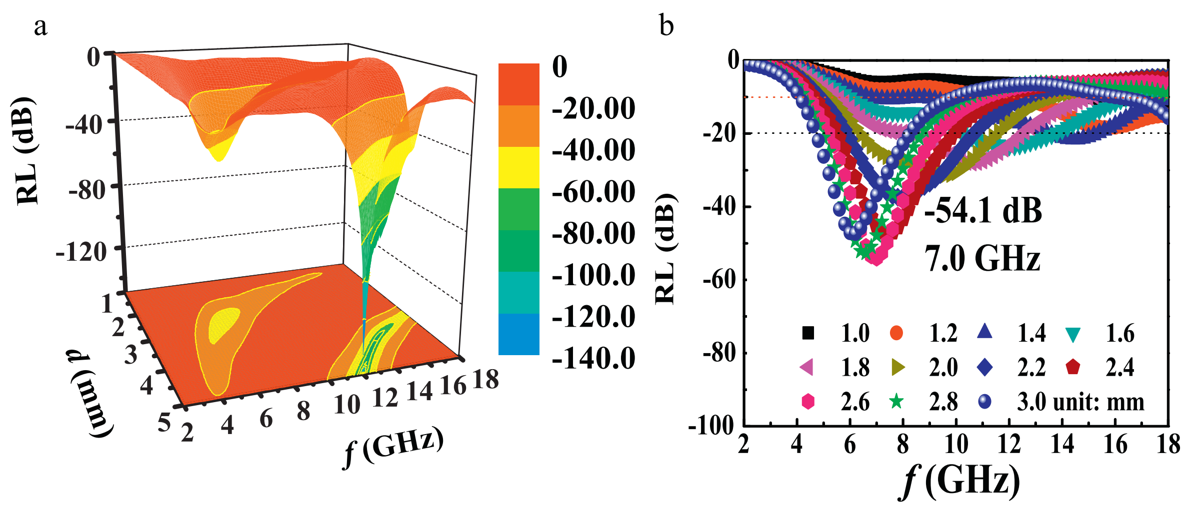

Fig. 3. RL of Fe(Mn)/Mn_7C_3/C-paraffin composites as a function of thickness and frequency: (a) three dimensional representation and (b) two dimensional representation.

exceeds −10 dB corresponding to 90% absorption, while BW_{-20} means the frequency interval where RL value exceeds −20 dB corresponding to 99% absorption. As shown in Fig. 3(a), an optimal RL of −142.1 dB, corresponding to almost 100% absorption, is observed at 12 GHz for 5.0 mm thickness layer, which is far bigger than the previous reported results. The intensity and the frequency at the reflection loss minimum depend on the properties and thickness of the materials [34]. It is worth noting that the number of dips increases with an increase in sample thickness. It can be seen that there is only one dip for 1–3 mm and the dip shifts to the lower frequency side with increasing thickness of the layer, while two complete dips can be observed for 3–5 mm. The occurrence of the dips is found to be due to a successive odd number multiple of the quarter wavelength (λ) thickness of the material or $d = n\lambda/4$ (n = 1, 3) [34].

The absorbing thickness of 5.0 mm is too thick for the rapid development in electronic industry. From the view point of practical use, the upper limit of absorbing thickness should be 3.0 mm. As shown in Fig. 3(b), BW_{-10} is 11.4 GHz (6.6–18 GHz) for the 1.4 mm thickness, which contains the whole X band (8–12 GHz), Ku band (12–18 GHz), and some of C band (6.6–8.0 GHz). BW_{-20} is 4.6 GHz (6–10.6 GHz) for the 2.2 mm thickness. An optimal RL reaches −54.1 dB at 7 GHz for 2.6 mm thickness. Compared with the Fe/SmO, Fe/C, Fe/SiO_2, Fe/ZnO, Fe/TiO_2, Fe(Mn)/ferrite nanocapsules, $CoFe_2O_4$/carbon nanotubes nanocomposites, Fe_3O_4/ZnO core/shell nanorods, and Fe_3O_4/TiO_2 core/shell nanotubes with a single thickness [16,19,20,23,35–39], BW_{-10} of Fe(Mn)/Mn_7C_3/C is sufficiently widened, due to the ternary dielectric relaxation and the enhanced natural resonance from the special core/shell/shell microstructure.

4. Conclusion

Fe(Mn)/Mn_7C_3/C nanocapsules have been synthesized by a modified arc discharge technique, with Fe(Mn) nanoparticles as the core, and Mn_7C_3 as the inner shell, and C as the outer shell. Fe(Mn)/Mn_7C_3/C nanocapsules have been exhibited the excellent microwave absorption properties at 2–18 GHz for thicknesses of 1.0–5.0 mm. An unusually high frequency (12 GHz) corresponding to the optimal RL (−142.1 dB) has been calculated for a layer with a thickness of 5.0 mm. BW_{-10} is 11.4 GHz (6.6–18 GHz) for 1.4 mm thickness, which contains the whole X band, Ku band, and some of C band. BW_{-20} is 4.6 GHz (6–10.6 GHz) for 2.2 mm thickness. The optimal RL and the broad bandwidth of RL qualify the Fe(Mn)/Mn_7C_3/C nanocapsules to be a prominent candidate for X–Ku band microwave absorption applications. The excellent microwave absorption properties result from the synergistic effect of double dielectric shells and soft magnetic cores.

Acknowledgments

This work was supported by The Hong Kong Polytechnic University Postdoctoral Fellowships Scheme (G-YX3 V) and National Basic Research Program (2010CB934603) of China, Ministry of Science and Technology of China.

References

[1] N. Li, Y. Huang, F. Du, X.B. He, X. Lin, H.J. Gao, Nano Lett. 6 (2006) 1141.
[2] R.C. Che, L.M. Peng, X.F. Duan, Q. Chen, X.L. Liang, Adv. Mater. 16 (2004) 401.
[3] J.C. Wang, C.S. Xiang, Q. Liu, Y.B. Pan, J.K. Guo, Adv. Funct. Mater. 18 (2008) 2995.
[4] X.F. Zhang, X.L. Dong, H. Huang, Y.Y. Liu, W.N. Wang, X.G. Zhu, B. Lv, J.P. Lei, C.G. Lee, Appl. Phys. Lett. 89 (2006) 053115.
[5] X.L. Shi, M.S. Cao, J. Yuan, X.Y. Fang, Appl. Phys. Lett. 95 (2009) 163108.
[6] Y.J. Chen, P. Gao, R.X. Wang, C.L. Zhu, L.J. Wang, M.S. Cao, J. Phys. Chem. C 113 (2009) 10061.
[7] W.F. Yang, L. Qiao, J.Q. Wei, Z.Q. Zhang, T. Wang, F.S. Li, J. Appl. Phys. 107 (2010) 033913.
[8] L. Qiao, X.H. Han, B. Gao, J.B. Wang, F.S. Wen, F.S. Li, J. Appl. Phys. 105 (2009) 053911.
[9] J.R. Liu, M. Itoh, K.I. Machida, Appl. Phys. Lett. 83 (2003) 4017.
[10] J.R. Liu, M. Itoh, K.I. Machida, Appl. Phys. Lett. 88 (2006) 062503.
[11] M.T. Sebastian, H. Jantunen, Int. J. Appl. Ceram. Tech. 7 (2010) 415.
[12] Y.L. Cheng, J.M. Dai, D.J. Wu, Z.R. Yang, Y.P. Sun, Nano. Res. Lett. 4 (2009) 1153.
[13] M. Terada, M. Itoh, J.R. Liu, K. Machida, J. Magn. Magn. Mater. 321 (2009) 1209.
[14] X.G. Liu, D.Y. Geng, H. Meng, W.B. Cui, F. Yang, Z.D. Zhang, Solid State Commun. 149 (2009) 64.
[15] J.R. Liu, M. Itoh, M. Terada, T. Horikawa, K.I. Machida, Appl. Phys. Lett. 91 (2007) 093101.
[16] X.G. Liu, D.Y. Geng, H. Meng, P.J. Shang, Z.D. Zhang, Appl. Phys. Lett. 92 (2008) 173117.
[17] Z. Han, D. Li, H. Wang, X.G. Liu, J. Li, D.Y. Geng, Z.D. Zhang, Appl. Phys. Lett. 95 (2009) 023114.
[18] X.G. Liu, Z.Q. Ou, D.Y. Geng, Z. Han, J.J. Jiang, W. Liu, Z.D. Zhang, Carbon 48 (2010) 891.
[19] X.F. Zhang, X.L. Dong, H. Huang, Y.Y. Liu, B. Lv, J.P. Lei, C.J. Choi, J. Phys. D: Appl. Phys. 40 (2007) 5383.
[20] L.G. Yan, J.B. Wang, X.H. Han, Y. Ren, Q.F. Liu, F.S. Li, Nanotechnology 21 (2010) 095708.
[21] X.G. Liu, D.Y. Geng, Z.D. Zhang, Appl. Phys. Lett. 92 (2008) 243110.
[22] X.G. Liu, D.Y. Geng, H. Meng, B. Li, Q. Zhang, D.J. Kang, Z.D. Zhang, J. Phys. D: Appl. Phys. 41 (2008) 175001.
[23] Z. Han, D. Li, X.G. Liu, D.Y. Geng, J. Li, Z.D. Zhang, J. Phys. D: Appl. Phys. 42 (2009) 055008.
[24] B. Lu, X.L. Dong, H. Huang, X.F. Zhang, X.G. Zhu, J.P. Lei, J.P. Sun, J. Magn. Magn. Mater. 320 (2008) 1106.
[25] X.G. Liu, Z.Q. Ou, D.Y. Geng, Z. Han, Z.D. Zhang, J. Phys. D: Appl. Phys. 42 (2009) 155004.
[26] X.G. Liu, X.H. Liu, Q. Zhang, Z.D. Zhang, J. Alloys Compd. 486 (2009) 14.

[27] X.G. Liu, S.W. Or, S.L. Ho, H. Wang, Z.D. Zhang, J. Alloys Compd. 509 (2011) 2929.
[28] X.G. Liu, D.Y. Geng, J.J. Jiang, Z.D. Zhang, J. Nanosci. Nanotechnol. 10 (2010) 2366.
[29] X.G. Liu, S.W. Or, E. Bruck, Z.D. Zhang, J. Nanopart. Res. 13 (2011) 1163.
[30] X.L. Dong, X.F. Zhang, H. Huang, F. Zuo, Appl. Phys. Lett. 92 (2008) 0132127.
[31] X.G. Liu, J.J. Jiang, D.Y. Geng, Z. Han, W. Liu, Z.D. Zhang, Appl. Phys. Lett. 94 (2009) 053119.
[32] F. Bødker, S. Mørup, S. Linderoth, Phys. Rev. Lett. 72 (1994) 282.
[33] C. Kittel, Phys. Rev. 73 (1948) 155.
[34] A.N. Yusoff, M.H. Abdullah, S.H. Ahmad, S.F. Jusoh, A.A. Mansor, S.A.A. Hamid, J. Appl. Phys. 92 (2002) 876.
[35] S. Sugimoto, T. Maeda, D. Book, T. Kagotani, K. Inomata, M. Homma, J. Alloys Compd. 330 (2002) 301.
[36] Q.A. Zhang, C.F. Li, Y.N. Chen, Z. Han, H. Wang, Z.J. Wang, Appl. Phys. Lett. 97 (2010) 133115.
[37] R.C. Che, C.Y. Zhi, C.Y. Liang, X.G. Zhou, Appl. Phys. Lett. 88 (2006) 033105.
[38] Y.J. Chen, F. Zhang, G.G. Zhao, X.Y. Fang, H.B. Jin, P. Gao, J. Phys. Chem. C 114 (2010) 9239.
[39] C.L. Zhu, M.L. Zhang, Y.J. Qiao, G. Xiao, F. Zhang, Y.J. Chen, J. Phys. Chem. C 114 (2010) 16229.